Submitted to ADVANCED MATERIALS

DOI: 10.1002/adma.

Tunnelling Negative Differential Resistance in a Flexible Active Composite

By *Samuel Littlejohn*, *Alain Nogaret*,* and *Simon Crampin*

[*] S. Littlejohn, Dr A. Nogaret, Dr S. Crampin

Department of Physics

University of Bath

Bath, BA2 7AY (United Kingdom)

Email: A.R.Nogaret@bath.ac.uk

Keywords:

Flexible electronics, Composite materials, Negative differential resistance, Graphene bilayer, Metal-insulator transition.

Developing flexible electronic materials with the ability to amplify signals is a major challenge for bioelectronics. Amplification is currently embodied by the transistor family and devices based upon negative differential resistance (NDR) that use band structure engineering to obtain a tunnelling current that decreases with increasing bias. The principles of NDR based oscillators,[1] amplifiers,[2] logic circuits[3] and their implementation on rigid substrates are now well established. The need for both intelligent sensor arrays that stretch like a skin and implantable control electronics is driving the search for novel soft conducting materials[4]. Stretchable interconnects[5-7] and flexible matrices have been obtained that exhibit pressure-sensing[8], temperature-sensing[9] and electroluminescent properties[10]. The next step in developing an active nervous system calls for a flexible electronic material that produces a signal gain. The ability to tune the electrical conductivity of the graphene bilayer[11-13] with an electric field provides a route for addressing this challenge through the generation of NDR.

Here we demonstrate a wide NDR region in the current-voltage characteristics of silicone filled with graphitic nanoparticles. At the peak, the conductor breaks up into domains of constant electric field separated by highly resistive domain boundaries. These are identified as individual graphite nanoparticles whose orientation in the electric field favours conduction across just two graphene layers. Large electric fields open a partial energy gap at the Fermi level which causes the current carrying bilayer to undergo a semimetal-to-insulator transition. The nucleation of highly resistive domain boundaries gives rise to the NDR. This picture explains the dependence of the *I-V* curves on the concentration of graphitic nanoparticles, temperature, channel length, as well as the disappearance of the NDR when the graphitic nanoparticles are replaced with amorphous carbon nanoparticles.

We formed graphite-silicone composites by mixing carbon nanoparticles in liquid silicone rubber, a low viscosity elastomer that is a perfect insulator at room temperature. Three allotropic forms of carbon were used to study the effect of the filler's crystallographic structure on the *I-V* curves of the composite. One composite was filled with nanoparticles of

highly oriented pyrolytic graphite averaging 450nm in length (**HOPG**). A second composite incorporated a*morphous carbon* nanoparticles of diameter 50nm (**AC**) and, the third composite was filled with *pyrolytic carbon* nanoparticles of diameter 50nm (**PC**) obtained by annealing **AC** nanoparticles at 1100°C for 1 hour in hydrogen. The crystallographic structure of all three allotropes was established by X-ray diffraction (supplementary information). The **HOPG** nanoparticles have graphene planes stacked in the two sequences ABA and ABC[14]. The **AC** nanoparticles are amorphous. In the **PC** nanoparticles, graphene layers grow with random orientations developing covalent bonds between layers. Ribbons of composite were moulded and cured on top of copper electrodes to perform four-terminal *I-V* measurements (**Figure 1b**). The *I-V* characteristics of **HOPG** and **PC** composites exhibit a transition from an Ohmic regime to a wide NDR region at higher bias (Figure 1a). The current peak that defines the transition is very robust as it survives millions of cycles of the bias voltage. The peak voltage is smaller in **PC** composites. In contrast, the **AC** composite shows no NDR and has conductivity three orders of magnitude lower than that of the **HOPG** and **PC** composites.

The dependence of the peak current on the **HOPG** filling fraction, p, is investigated in **Figure 2a**. A systematic shift in the peak position from 12V at 34.2% to 115V at 25.6% occurs while the zero bias conductivity drops from σ_0=8mS to 0.06mS. The composite becomes insulating at a critical filling fraction of p_c=24%, above which the conductivity follows a power law $\sigma_0 \sim (p - p_c)^4$ characteristic of percolation through the network of nanoparticles[15] (Figure 2b). The current peak in the **PC** composite exhibits a similar shift to higher bias when the filler fraction decreases (Figure 2e). To investigate the possibility that the NDR might be due to silicone going through its glass transition at ~166K, we measured the composite temperature in-situ while recording the *I-V* curves. To do this, we inserted a Pt temperature sensor inside the composite. Joule heating was found to increase the sample temperature from 77K to 81K (Figure 2f) which is well below the glass transition temperature

of silicone. Hence, the current peak cannot be attributed to any structural transition in silicone induced by Joule heating.

The *I-V* curves are next measured over different lengths of composite (Figure 2g). The peak voltage increases linearly with the voltage probe separation (Figure 2h). This demonstrates that the electric field is spatially homogeneous up to the peak where it reaches its maximum value F_p determined by the slope. After the current has peaked, the NDR only appears in ribbons longer than 0.6mm. Over shorter distances, the current increases up to the peak value of previous curves but then decreases, retracing the *I-V* curve while the two terminal bias voltage (across the current contacts) is still increasing. This behaviour can only be explained by the sample fragmenting into *domains of constant electric field* at the peak[16]. The domains develop highly resistive boundaries that sustain the extra voltage seen in the NDR region and account for the drop in current.

The presence of a NDR region in both **HOPG** and **PC** composites but not in the **AC** composites links the NDR to conduction through the graphitic planes. By considering the percolation path in **Figure 3a** (see also supporting material Figure S1), we demonstrate that, for the majority of **HOPG** nanoparticles, the current flows inside just one graphene plane. In the remaining nanoparticles, the current jumps one interlayer spacing and rarely more. Whether a nanoparticle conducts through a graphene monolayer, bilayer or trilayer depends upon the angle θ between its planes and the electric field. Using Ohm's law $\vec{j} = \vec{\sigma}\vec{E}$ we determine the angle φ between the current density and the graphite planes. The number of graphite interlayers, *N*, between the current entry point A and exit point B of the nanoparticle is then found in terms of the ratio of the in-plane to perpendicular conductivity of graphite[17], $\sigma_{\parallel}/\sigma_{\perp} = 3000$, the distance between graphite planes *c*=0.335nm and the average length of a HOPG nanoparticle *l*=450nm. Using the construction in Figure.3b, we obtain $N = \frac{l}{c}\frac{\sigma_{\perp}}{\sigma_{\parallel}}\tan\theta \cong 0.441\tan\theta$. Therefore, when θ is between 0 and 66°, HOPG nanoparticles

conduct through a single graphite monolayer (N<1). Between 66° and 78° conduction is through a graphite bilayer (N<2), between 78° and 82° a graphite trilayer and so on. Since **HOPG** particles assume random orientations in the matrix, 93.5% of them remain semi-metallic at any value of the electric field. In the remaining 6.5%, the current flows into the nanoparticle through one graphite layer (point A), then crosses one interlayer before exiting through the adjacent graphite layer (point B). The (mostly) transverse bias V_{AB} opens a partial energy gap at the Fermi level in graphite. This gap is shown in the local density of states plots of Figure 3c. Unlike the gap of the free standing graphene bilayer,[11-13] the gap of the embedded bilayer opens above a threshold $V_{AB} > 2\gamma_2$ corresponding to the energy overlap of the π-band ($2\gamma_2$=40meV). The gap is partial. Nevertheless it is sufficiently well defined to induce a semimetal-insulator transition since the density of states at the Fermi level drops from 100% at 0V to just 3% at 0.6V. We conclude that nanoparticles tilted at an angle between 66° and 78° develop a high resistance that breaks the composite into domains of constant electric field (F_p).

We model the *I-V* curve of one such nucleation site in Figure 2c and show that it accounts for the observed NDR. Consider the conduction band of the graphite-silicone-graphite junction in Figure 2d. At small bias the emitter particle is semi-metallic ($V_{AB} \cong 0$) and the silicone barrier is insulating ($V_{BC} \cong V$). Increasing V increases the Fowler-Nordheim tunnelling current which gives the Ohmic region of the *I-V* curves. Near the peak, the resistance of the tunnelling barrier drops to the level of the resistance of the emitter. At this point V_{AB} starts to increase while V_{BC} saturates. This trend is reinforced by the opening of the energy gap at the Fermi level, which reduces the density of thermal carriers in the biased graphite bilayer. The resistance of the emitter increases sharply giving the NDR (Figure 2c). Decreasing the **HOPG** filler fraction has the effect of increasing the tunnelling barrier width b. The peak current shifts to higher V for the simple reason that thicker barriers require more

bias to match their resistance to that of the emitter. We estimate the width of the tunnel barrier from the filler fraction through $b = l[(\pi/6p)^{1/3} - 1]$. Then b increases from 67nm at p=34.5% to 139nm at p=21%. The good agreement between Figures 2a and 2c supports the hypothesis that the NDR originates from a field induced semimetal-insulator transition in embedded graphene bilayers.

The temperature dependence of the *I-V* curves is shown in Figure 3d. The most notable feature is the shift of the current peak from a finite bias voltage at 4K to 0V at ~200K. The peak position has a temperature dependence which is independent of the graphite filling fraction (Figure 3e). The main effect of temperature is to activate a thermal current above the silicone tunnel barrier lowering its resistance. The effect on the peak position is similar (but not identical) to the effect of increasing the graphite filler fraction. We have calculated the temperature dependence of the peak position using the silicone barrier height ϕ_0 as the adjustment parameter. The effects of phonon scattering on the mobility of graphite[17] and the thermal activation of carriers[18] were included in the tunnelling model. The theoretical peak positions for barrier heights ranging from 50meV to 250meV are plotted in Figure 3e (full lines) from which we extract a best fit of ϕ_0=165meV. Below 166K, bulk silicone is in its glass state. The frozen matrix explains why the zero bias conductivity σ_0 is the same for all *I-V* curves below 174K. Above 166K, silicone is in the rubber state. The tunnelling barriers can now expand under Joule heating[15,19]. This explains why σ_0 is halved in the 195K and 206K curves.

To conclude, using benchtop chemistry, we have demonstrated a flexible material, incorporating graphite nanoparticles in silicone that may be used for making electronic amplifiers. We have already demonstrated a flexible electronic oscillator by embedding a composite device in a resonating circuit, see supplementary information. Given the present state of the art, it seems unlikely that polymer amplifiers will compete with semiconductor

amplifiers on speed, nonetheless they do present major advantages over the latter. These include the conformability and biocompatibility conferred by silicone, the dramatic reduction of material and fabrication costs over semiconductor tunnel devices, scalability and a peak-to-valley current ratio without upper theoretical limit. The noise seen in the *I-V* curves beyond the peak is believed to result from the shutting off of percolation paths and their re-routing around the graphite nanoparticles that have developed an insulating behaviour. This noise can be reduced by engineering the orientation of nanoparticles with respect to the electric field. Although, we have demonstrated the NDR below 200K, Figure 3e suggests that room temperature operation will be achieved by increasing the barrier height to ~250meV by tuning the chemical affinity of the elastomer. On the effects of mechanical strain, the effect of hydrostatic pressure on the NDR is similar to increasing the filler fraction, see supplementary information Figure S13. The exceptional width of the NDR region however warrants stable amplification when the device is deformed.

EXPERIMENTAL INFORMATION

Device fabrication: Graphite-silicone composites were prepared by mixing carbon nanoparticles (Nanoamor 450nm, Aldrich 50nm) in liquid silicone rubber (Alchemie RTV139). The nanoparticles were incorporated into the liquid silicone through an extended mixing process. RTV catalyst (C148) was added to the mixture in a ratio of 1:10. The mixture was moulded at the surface of a printed circuit board and left to cure at room temperature for 24hrs. The volume fraction, p, of the filler was determined from the filler weight fraction and the tabulated values of the densities of graphite and liquid silicone. The contact resistance of the copper / HOPG composite interface was 500Ω at p=28%. A Pt temperature sensor of dimensions 1.2mm×1.6mm×0.8mm (Innovative Sensor Technnologies) was embedded inside the composite to record the elevation of temperature induced by Joule heating.

Band structure calculations: The band structure of the embedded graphene bilayer was modelled using the tight binding method. The bias V_{AB} was applied between layers 48 and 49 at the centre of a stack of 96 graphite layers. The outcome of the tight binding calculations was compared to ab-initio density functional theory using both GGA and hybrid B3LYP functionals in the case of the free-standing graphene bilayer and trilayer. The three methods give similar band energies within ±0.3eV of the Fermi level. The local density of states was taken on the non overlapping carbon atoms of the hexagonal unit cell at coordinates $\left(\frac{1}{3},\frac{2}{3},0\right)$ and $\left(\frac{2}{3},\frac{1}{3},\frac{1}{2}\right)$. These atoms couple through γ_2 and give the main contribution to the carrier states along the c-axis of graphite. We averaged the LDOS over the in-plane momentum of thermal electrons at the Dirac point.

SUPPORTING INFORMATION

Supporting Information is available online from Wiley InterScience or from the author.

Received: ……..

Revised: ……..

Published online: ……..

REFERENCES

[1] E. R. Brown, J. R. Söderström, C. D. Parker, L. J. Mahoney, K. M. Molvar, T. C. McGill, *Appl. Phys. Lett.* **2004**, *58*, 2291.

[2] W. F. Chow, *Principles of Tunnel Diode Circuits*, Wiley, New York **1964**.

[3] F. Capasso, S. Sen, F. Beltram, L. M. Lunardi, A. S. Vengurlekar, P. R. Smith, N. J. Shah, R. J. Malik, A. Y. Cho, *IEEE. Trans. on Elect. Dev.* **1989**, *36*, 2065.

[4] J. A. Rogers, T. Someya, Y. Huang, *Science* **2010**, *327*, 1603.

[5] K. S. Kim, Y. Zhao, H. Jang, S. Y. Lee, J. M. Kim, K. S. Kim, J. –H. Ahn, P. Kim, J. -Y. Choi, B. H. Hong, *Nature* **2009**, *457*, 706.

[6] T. Sekitani, H. Nakajima, H. Maeda, T. Fukushima, T. Aida, K. Hata, T. Someya, *Nature Mat.* **2009**, *8*, 494.

[7] D. –Y. Khang, H. Jiang, Y. Huang, J. A. Rogers, *Science* **2006**, *311*, 208.

[8] T. Someya, T. Sekitani, S. Iba, Y. Kato, H. Kawaguchi, T. Sakurai, *Proc. Nat. Acad. Sci.* **2004**, *101*, 9966.

[9] T. Someya, Y. Kato, T. Sekitani, S. Iba, Y. Noguchi, Y. Murase, H. Kawaguchi, T. Sakurai, *Proc. Nat. Acad. Sci.* **2005**, *102*, 12321.

[10] H. Stirringhaus, N. Tessler, R. H. Friend, *Science* **1998**, *280*, 1741.

[11] T. Ohta, A. Bostwick, T. Seyller, K. Horn, E. Rotenberg, *Science* **2006**, *313*, 951.

[12] K. S. Novoselov, E. McCann, S. V. Morozov, V. I. Fal'ko, M. I. Katsnelson, U. Zeitler, D. Jiang, F. Schedin, A. K. Geim, *Nature Phys.* **2006**, *2*, 177.

[13] E. McCann, V. I. Fal'ko, *Phys. Rev. Lett.* **2006**, *96*, 086805.

[14] H. Lipson, A. R. Stokes, *Proc. Roy. Soc. London A* **1942**, *181*, 101.

[15] J-. C. Huang, *Adv. Polymer Tech.* **2002**, *21*, 299.

[16] H. T. Grahn, R. J. Haug, W. Müller, K. Ploog, *Phys. Rev. Lett.* **1991**, *67*, 1618.

[17] M. S. Dresselhaus, G. Dresselhaus, *Adv. in Phys.* **2002**, *51*, 1.

[18] R. Tsu, L. Esaki, *Appl. Phys. Lett.* **1973**, *22*, 562.

[19] J. Zhang, S. Zhang, S. Feng, Z. Jiang, *Polym. Int.* **2005**, *54*, 1175.

FIGURE CAPTIONS

Figure 1. (a) *I-V* characteristics of silicone-HOPG, silicone-AC and silicone-PC composites. **(b)** Silicone-HOPG ribbon fabricated at the surface of copper electrodes. The *I-V* curves are measured in the four terminal configuration. The composite ribbon shown is 125±25μm thick, 1.8±0.2mm wide.

Figure 2. (a) Dependence of the *I-V* curves on the volume fraction p of HOPG nanoparticles. **(b)** Zero-bias conductivity plotted against p-p_c where p_c is the graphite fraction at the threshold of conduction. The zero-bias conductivity follows a percolation power law $\sigma_0 \sim (p - p_c)^4$ (dashed line). **(c)** Theoretical *I-V* curves of the graphite-silicone-graphite tunnel barrier shown in **(d)**. Below the peak, the tunnelling current increases with V. Above the peak, V opens an energy gap in the emitter which sharply increases its resistance. **(e)** *I-V* curves of the silicone-PC composite. **(f)** Joule heating inside the composite recorded while measuring *I-V* curves. The effect of the bias ramp rate is shown. **(g)** Dependence of the *I-V* curves on the length of the composite. Sections of sample longer than 0.6mm exhibit a NDR. Shorter sections show no NDR in 6 out of the 7 samples studied. Instead, the voltage increases up to the peak and decreases again (arrows). **(h)** Dependence of the peak voltage on the length of the composite. The electric field is homogeneous across the device up to a maximum value of F_p=20kV.m^{-1} (HOPG) and F_p=12kV.m^{-1} (PC).

Figure 3. (a) Percolation path through randomly oriented HOPG nanoparticles (blue line). Particles 1, 2 and 4 have graphite planes tilted by less than 66° from the electric field direction and are semi-metallic. Particles tilted between 78° and 90° have a very high resistance which is short-circuited by the percolation path. Particles with intermediate tilt angles, such as particle 3, undergo a semimetal-to-insulator transition as V_{AB} biases just one graphite bilayer.

When $F>F_p$, particles of type 3 develop a high resistance which breaks the percolation path into domains of constant electric field F_p. **(b)** Current density and electric field inside particle 3. **(c)** The local density of states (LDOS) of a graphite crystal as a function of the layer number. V_{AB} is applied between layers 48 and 49. V_{AB} opens a partial energy gap in the π-band at the Fermi level (E=0). **(d)** Temperature dependence of the I-V curves of a HOPG composite. **(e)** Temperature dependence of the peak position for p=32% (squares) and p=28% (circles) compared to the theoretical temperature dependences calculated for different heights of the tunnelling barrier (full lines). The best fit to the data is for a barrier height ϕ_0=165meV (red line).

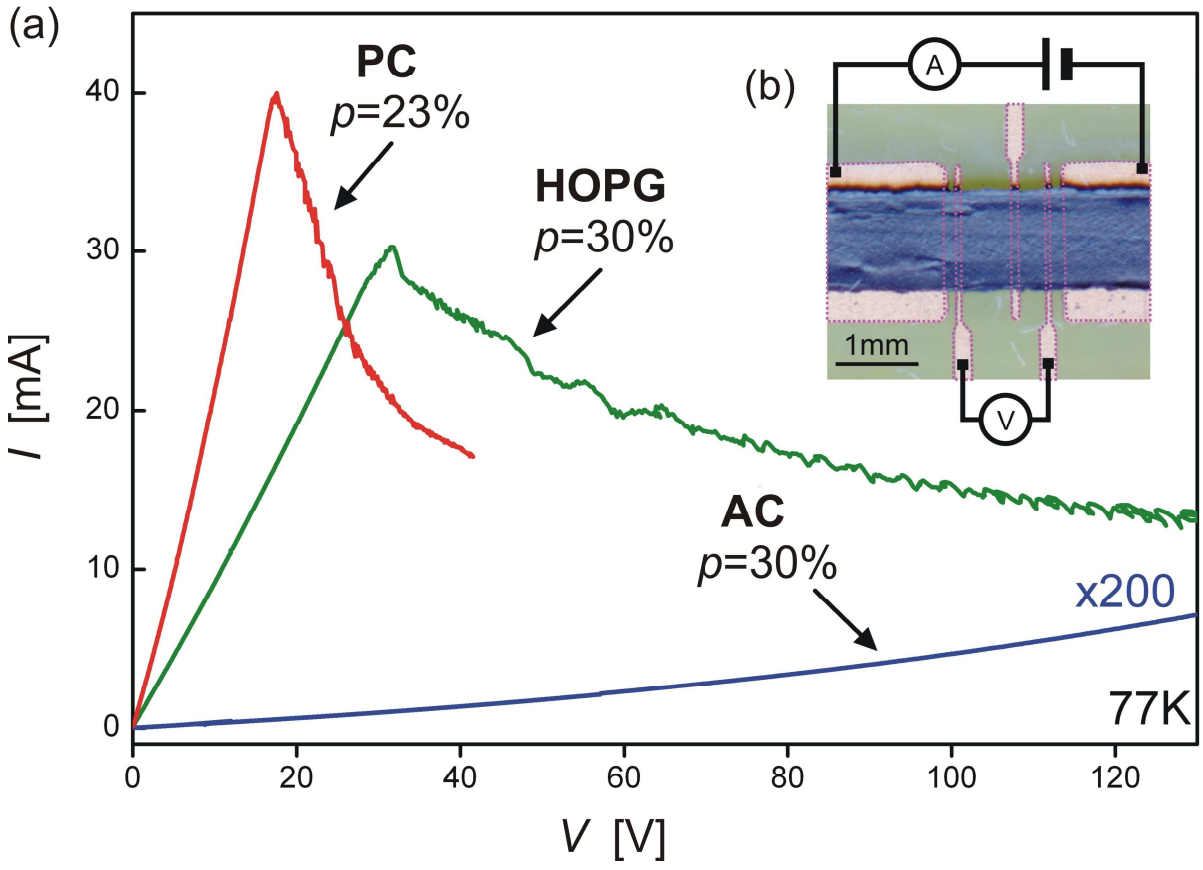

FIGURE 1

Littlejohn *et al.*

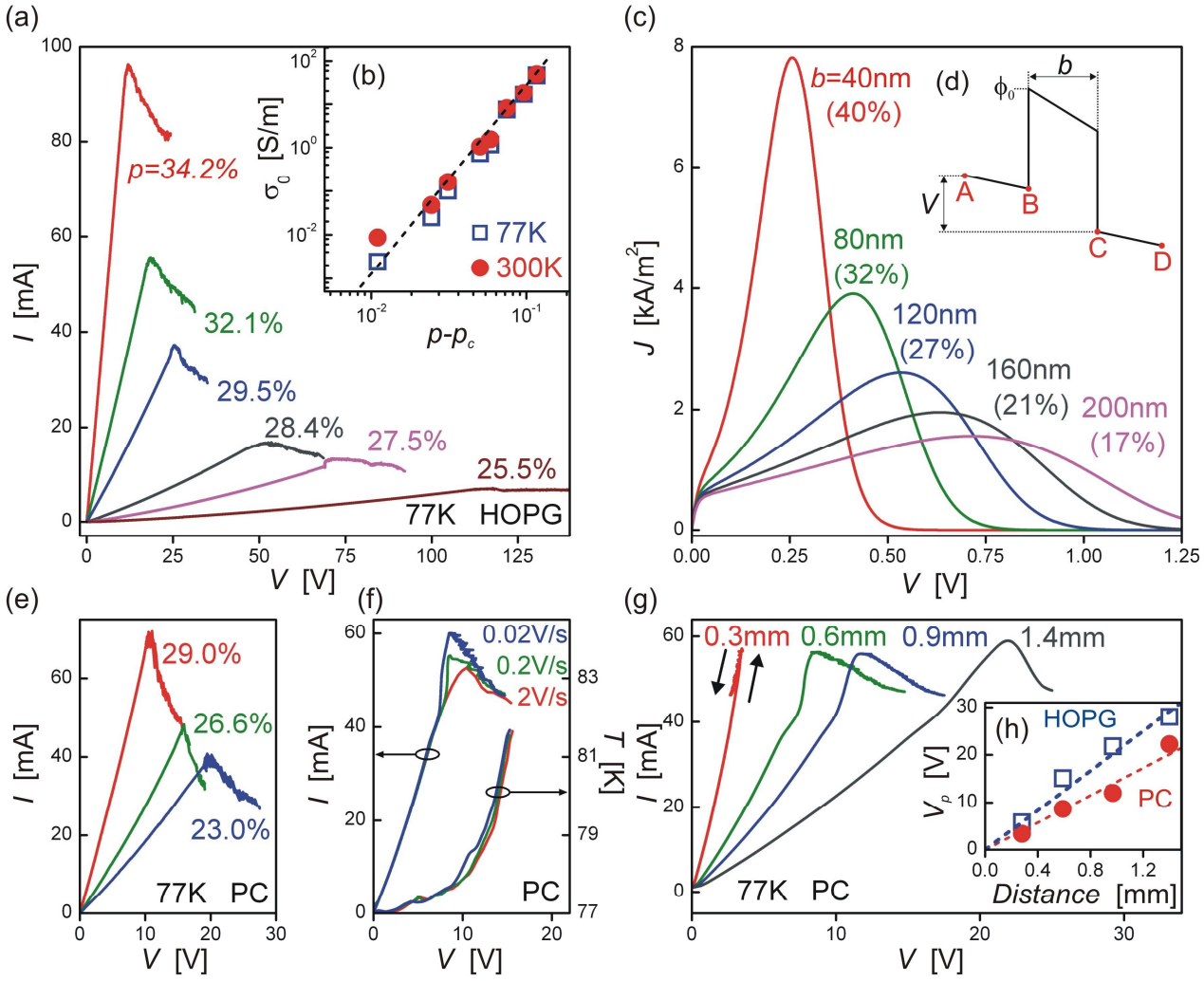

FIGURE 2

Littlejohn *et al.*

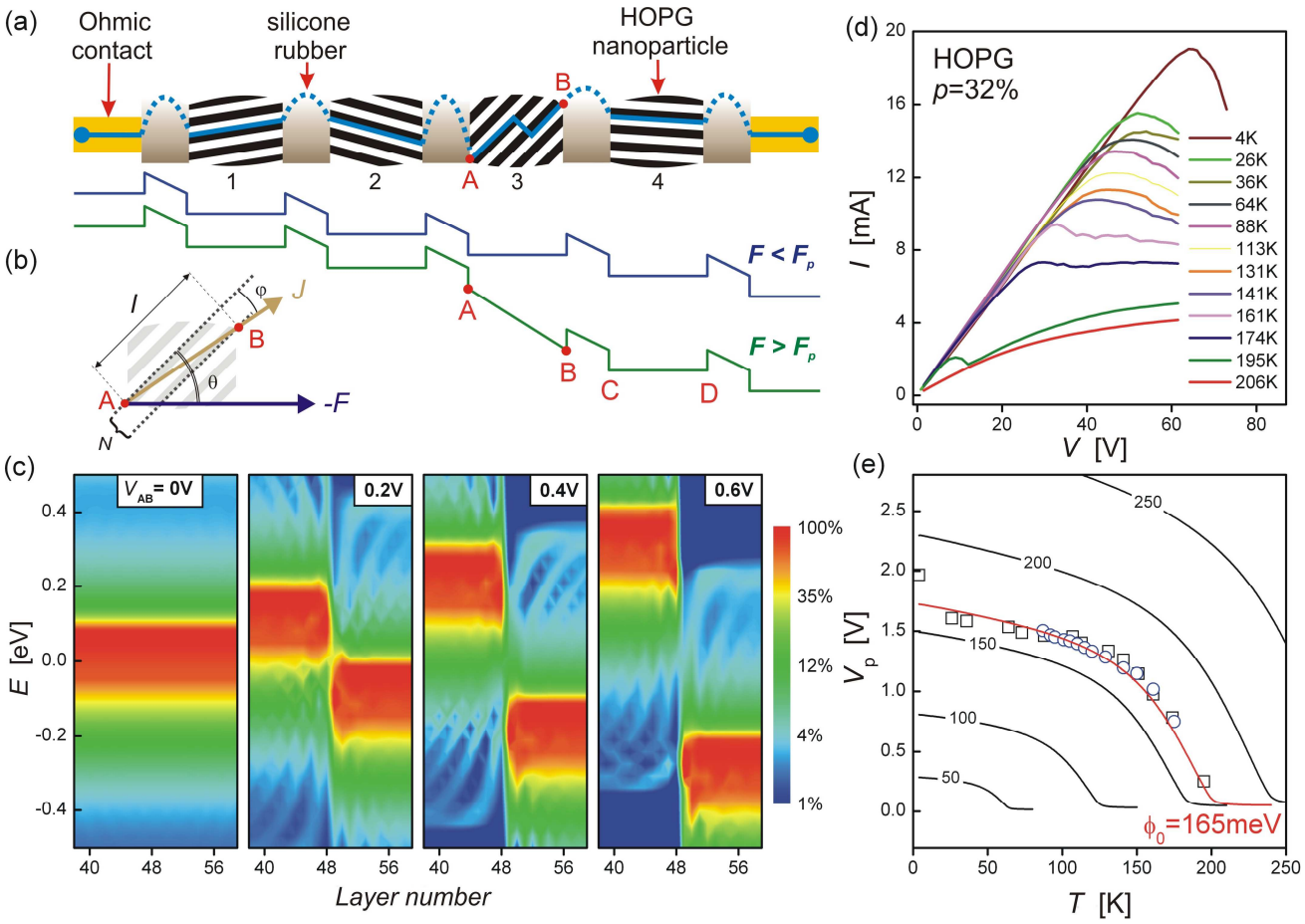

FIGURE 3

Littlejohn *et al.*

TABLE OF CONTENTS

Tunnelling Negative Differential Resistance in a Flexible Active Composite

Authors: Sam Littlejohn, Alain Nogaret, and Simon Crampin

Keywords: Flexible electronics, Composite materials, Charge transport

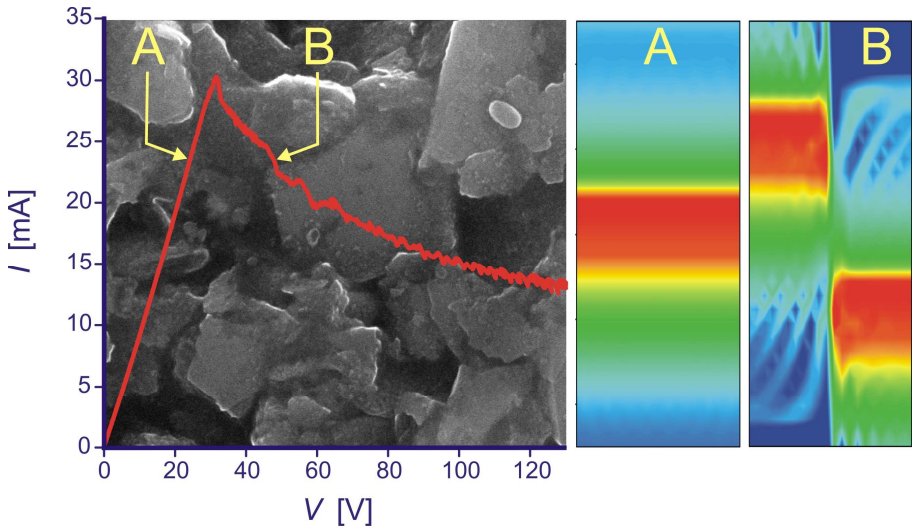

Entry: **A novel type of negative differential resistance** is demonstrated in composites incorporating graphite nanoparticles in a silicone matrix. The NDR occurs as the electric field breaks the π band of graphite initiating a semimetal to insulator transition. The current peak is robust and tuneable with the graphite concentration. This material can produce flexible electronic amplifiers for bioelectronic applications.

SUPPORTING MATERIAL

Tunnelling Negative Differential Resistance of Flexible Active Composite

SUMMARY

I. MATERIAL CHARACTERIZATION

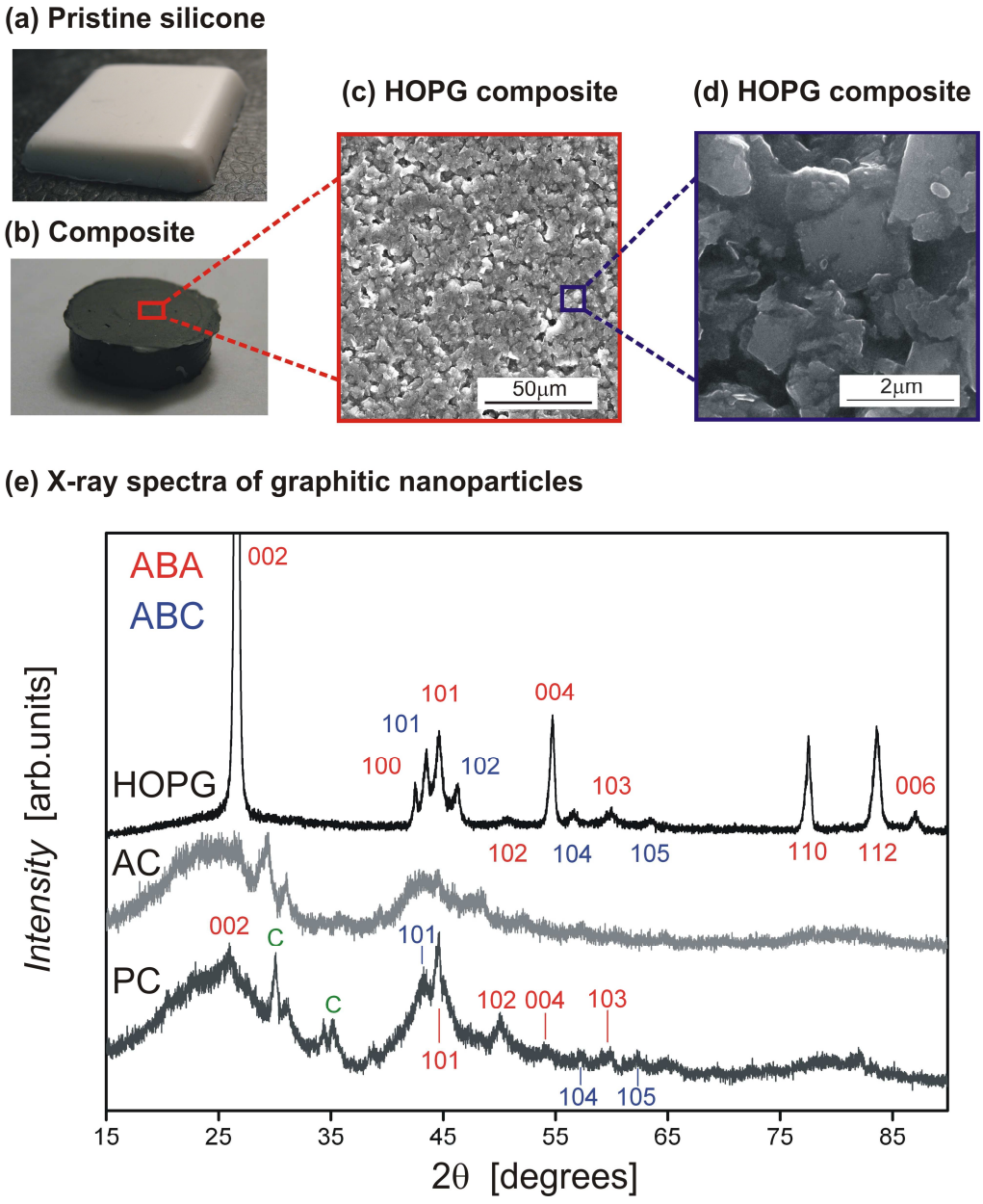

Figure S1 – **SEM micrographs of the HOPG composite and X-ray diffraction spectra**

(a) Pristine silicone rubber (Alchemie RTV 139).

(b) Conductive silicone rubber obtained by mixing in **HOPG** nanoparticles.

(c) SEM micrograph the **HOPG** composite showing an isotropic and homogeneous texture.

(d) Higher resolution SEM image of the **HOPG** composite showing the facets of individual nanoparticles i.e. the orientation of the graphite planes. The average particle size is 450nm. At the edges of nanoparticles the white lines represent the insulating silicone film that enhances the natural SEM contrast at the edges. The silicone thickness is 50-100nm.

(e) XRD of graphite nanoparticles (**HOPG**), amorphous carbon nanoparticles (**AC**) and pyrolytic carbon nanoparticles (**PC**). The **HOPG** nanoparticles have graphene planes stacked in the two sequences ABA and ABC as evidenced by the (101) doublet. The **AC** nanoparticles are amorphous. The **PC** nanoparticles develop sp^2 covalent bonds as indicated by the resurgence of the (101) peaks. Their graphene layers however have random orientations as evidenced by the faint main diffraction peak. Covalent bonds between the graphene planes give rise to peaks **C**.

II. FLEXIBLE ELECTRONIC OSCILLATORS MADE OF GRAPHITE-SILICONE

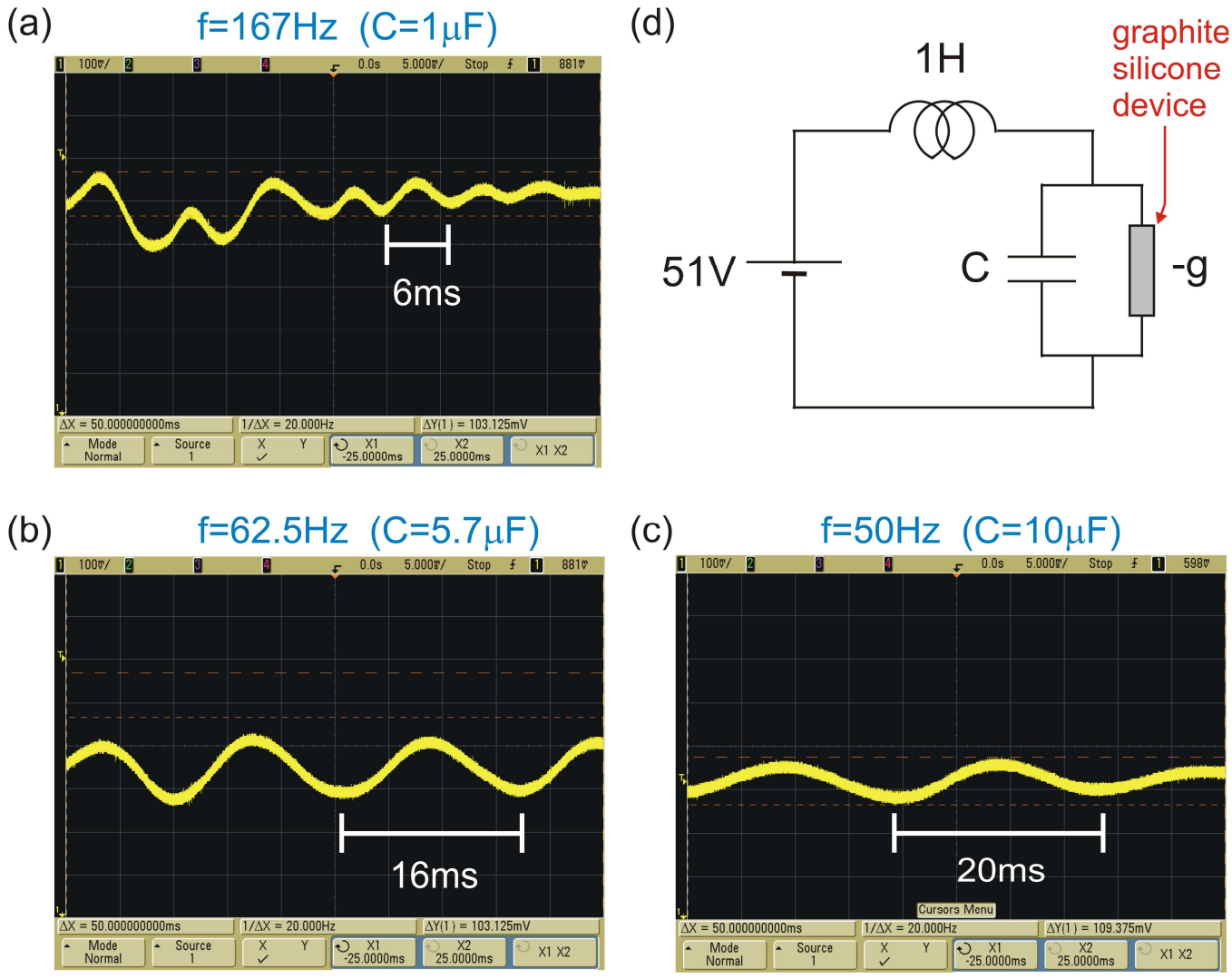

Figure S2 – **Demonstration of flexible electronic oscillators**

(a) Spontaneous voltage oscillations develop across the HOPG composite device when it is biased in the NDR region. With a capacitance C=1μF the oscillator generates a frequency of 167Hz.

(b) Spontaneous oscillations at 62.5Hz (C=5.7μF).

(c) Spontaneous oscillations at 50.0Hz (C=10μF).

(d) The composite device is embedded in the resonating circuit pictured. The circuit outputs an alternating voltage at frequency $f = 1/2\pi\sqrt{LC}$ which is currently tuneable in the range 10-250Hz.

III. FORMATION OF ELECTRIC FIELD DOMAINS

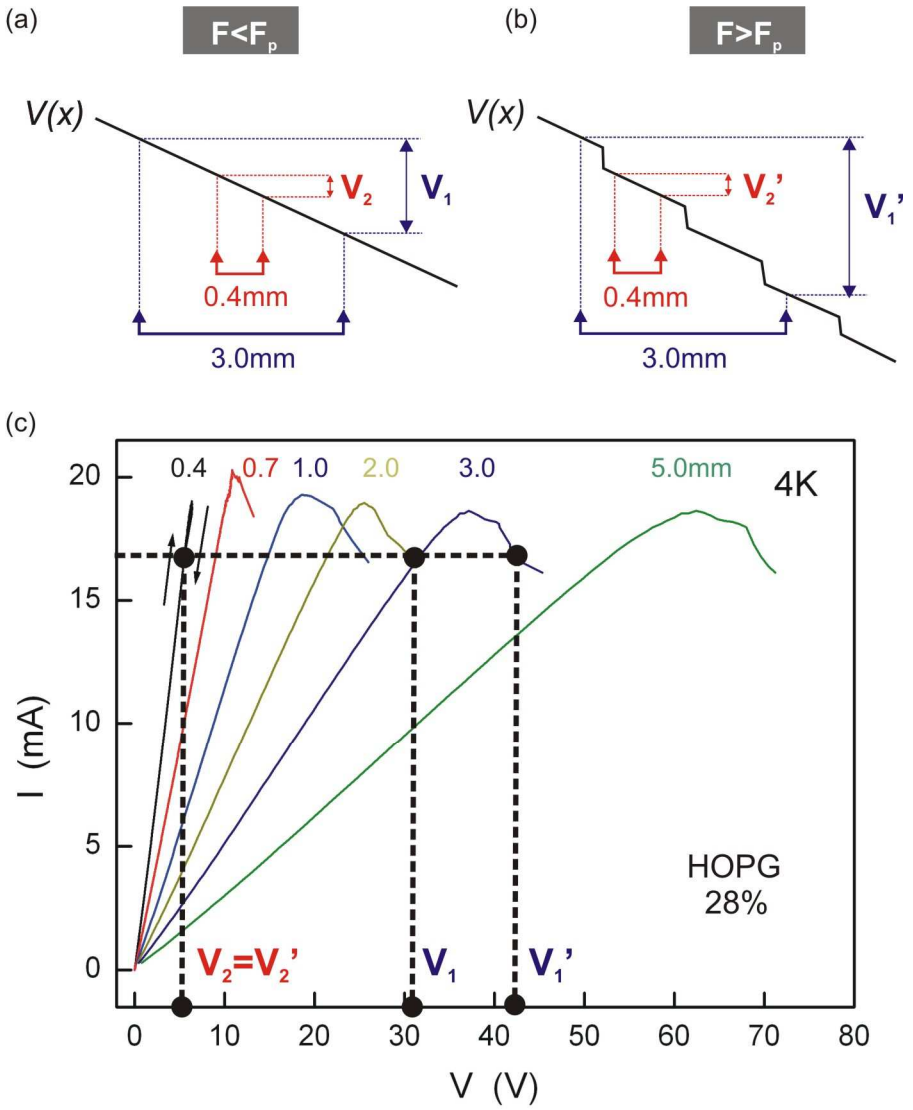

Figure S3 – **Effects of the formation of electric field domains on the *I-V* curves**

(a) *Before the current peak*, the electric field is constant over the length of the composite.

(b) *Above the current peak*, the composite breaks into ***domains of constant electric field*** separated by highly resistive boundaries. These boundaries are individual graphite nanoparticles which develop a semimetal-insulator transition. If the current-voltage characteristic is measured on a scale larger than the size of an electric field domain, one observes an extra voltage dropped across the ***highly resistive domain boundaries***. The *I-V* curve across a domain boundary has a NDR region that we calculate in Figure.2c and that we observe here over sample lengths >0.7mm – see panel (c). If the resistance is measured within one electric field domain, it remains the same before and after the peak. This behaviour is observed over the 0.4mm probe separation – see panel (c).

(c) Current voltage characteristics of the HOPG composite measured across voltage probe separations of 0.4mm, 0.7mm, 1mm, 2mm, 3mm and 5mm.

IV. MODELLING THE *I-V* CURVE OF THE GRAPHITE-SILICONE SYSTEM

Transmission coefficient through the silicone tunnel barrier:

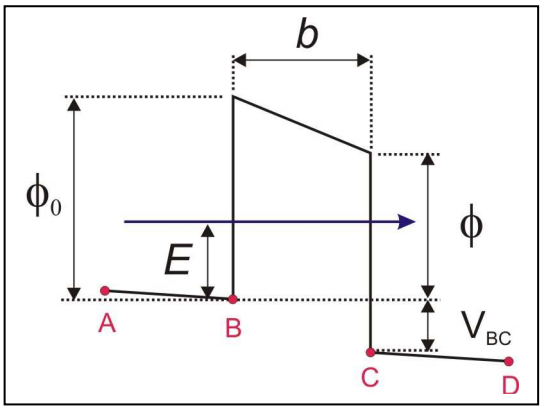

$$T(E,V_{BC}) = \exp\left(-4\frac{\sqrt{2m^*}}{3\hbar eF}\Phi\right)$$

$$\Phi \equiv \begin{cases} (\phi_0 - E)^{3/2} & \phi < E < \phi_0 \\ (\phi_0 - E)^{3/2} - (\phi - E)^{3/2} & E < \phi \end{cases}$$

$b \equiv$ barrier width — $E \equiv$ electron energy
$V_{BC} \equiv$ barrier bias — $F = V_{BC}/b$
$\phi_0 \equiv$ barrier height — $\phi_0 = \phi + V_{BC}$
AB = graphite emitter
BC = silicone tunnel barrier

(i) The **current density through the silicone tunnel barrier** is obtained by integrating $T(E,V_{BC})$ over the emitter states of the graphite nanoparticle. We note γ_1 the coupling between nearest neighbour graphite atoms in the plane, $v_F \approx 10^6\, m.s^{-1}$ the electron velocity at the Dirac point and $m^* = \gamma_1/(2v_F^2)$ the effective mass of electrons in the emitter. The density of tunnelling current[1] is:

$$J = \frac{e\gamma_1 k_B T}{(2\pi)^2 \hbar^3 v_F^2}\int_0^\infty T(E,V_{BC})F(E,T,V_{BC},V_{AB})\,dE$$

$$F(E,T,V_{BC},V_{AB}) = \ln\left[\frac{1+\exp\{-\beta(E+eV_{AB}/2)\}}{1+\exp\{-\beta(E+eV_{AB}\sin\varphi/2+eV_{BC})\}}\right] \qquad \text{(S1)}$$

Eq.S1 incorporates both the thermally activated and the tunnelling currents. The supply function, $F(E,T,V_{BC},V_{AB})$ accounts for the thermo-activated current (T dependence), the blockade of tunnelling by occupied collector states (V_{BC} dependence) and the opening of an energy gap in the graphite emitter induced by the electric field (V_{AB} dependence). Eq.S1 assumes coherent tunnelling.

(ii) The **current density through the graphite emitter** is obtained as follows. Consider one graphite nanoparticle in the silicone matrix - see Fig.3(b). We note θ the angle between the applied electric field and the graphite planes, φ the angle between the vector current density and the graphite planes. The current density is given by Ohm's law $\vec{j} = \vec{\vec{\sigma}}\vec{E}$. As is well known, graphite favours conduction in the graphite planes with a ratio of the in-plane to the perpendicular conductivity[2] of $\sigma_{\parallel}/\sigma_{\perp} = 3000$. The current density is $j_{\parallel} = \sigma_{\parallel}E_{\parallel}$ and $j_{\perp} = \sigma_{\perp}E_{\perp}$. Writing $j_{\perp}/j_{\parallel} = \tan\varphi$ and $E_{\perp}/E_{\parallel} = \tan\theta$, one obtains:

$$\tan\varphi = \frac{\sigma_{\perp}}{\sigma_{\parallel}}\tan\theta \cong \frac{1}{3000}\tan\theta \qquad \text{(S2)}$$

The number of graphite interlayers crossed between A and B is:

$$N = \frac{l}{c}\frac{\sigma_{\perp}}{\sigma_{\parallel}}\tan\theta \qquad \text{(S3)}$$

where c=0.335nm is the distance between graphite planes and l=450nm is the average length of graphite nanoparticles. Eq.S3 is plotted in Fig.S4 below.

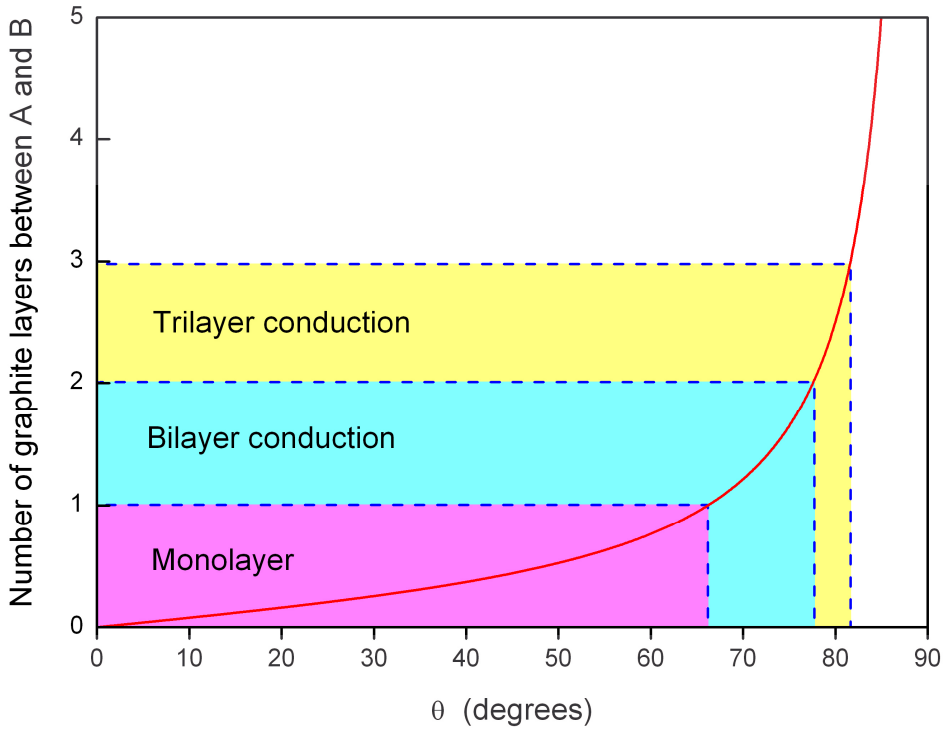

Figure S4 – Number of graphite interlayers between the current entry point A and the current exit point B as a function of the tilt angle of the electric field away from the graphite plane, θ. Angles between 0-66° see conduction through ***one graphite monolayer***; between 66°-78° conduction is through a ***graphite bilayer***, between 78°-82° a ***graphite trilayer*** etc.

The ***metal-insulator transition takes place in the nanoparticles whose orientation favours bilayer conduction between 66° and 78°***. The metal insulator transistor may also occur in trilayers if the stacking is rhombohedral and the bias V_{AB} is twice higher than that of the bilayer – see section VI. These extra requirements mean that the metal-insulator transition is less likely to occur in trilayers.

The current density of bilayer graphene is given by[3]:

$$J = \frac{e^2}{h}\frac{\gamma_1 k_B T}{u_0^2}\frac{V_{AB}\cos\varphi}{l}\frac{150^{1.2}}{T^{1.2}+150^2}\int_0^{\infty} dx \frac{1}{1+\exp\left(x + eV_{AB}\sin\varphi/2k_B T\right)} \qquad \text{(S4)}$$

where u_0 is the strength of the scattering potential. A value of $u_0 \approx 1$ meV for the interaction potential with impurities is obtained from the conductivity of graphene[4] at 4K. Increasing the temperature reduces

the density of thermal carriers n across the gap – see the integral term in Eq.S4. At higher temperature, electron-phonon scattering[2,5] reduces the mobility in the graphite planes according to $\mu \propto T^{-1.2}$. We have included the prefactor $\mu(T)/\mu(0) = 150^{1.2}/(T^{1.2}+150^{1.2})$ which fits the experimental mobility data of Sugihara et al.[5].

(iii) We apply the current conservation law, equating Eqs.S1 and S4 to find the relationship between the ***potential dropped across the tunnelling barrier*** V_{BC} and the ***potential dropped across the graphite emitter*** V_{AB}. The equation is solved numerically. V_{AB} and V_{BC} are plotted as a function of $V=V_{AB}+V_{BC}$ in Fig.S5.

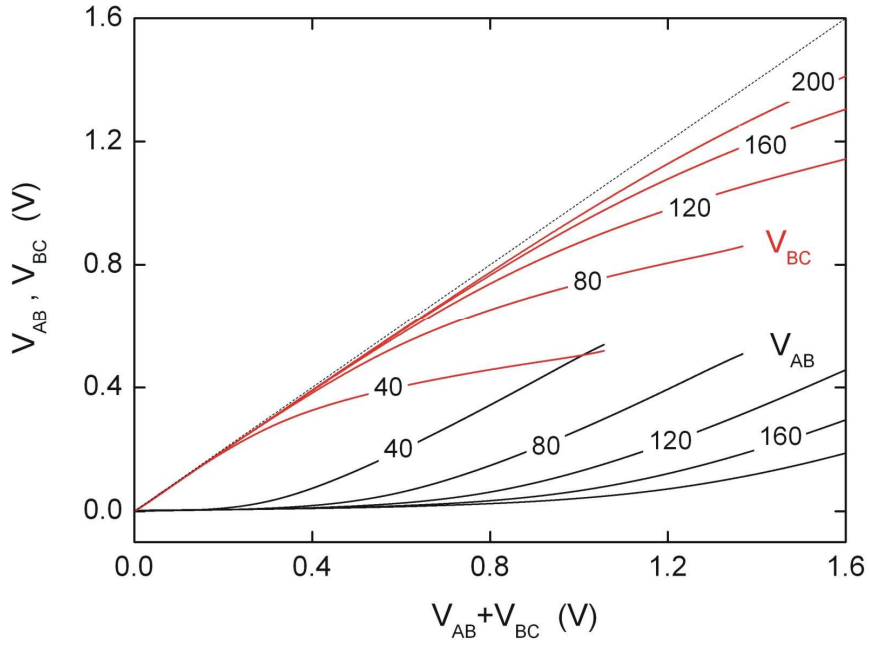

Figure S5 – Redistribution of bias V between the emitter (V_{AB}) and the barrier (V_{BC}).
At low bias V, graphite is semi-metallic, silicone is an insulator. The applied bias is all dropped across the silicone layer giving $V_{BC} \approx V$ (red curve) and $V_{AB} \approx 0$ (black curve).
At higher bias V, the silicone tunnelling barrier becomes increasingly transparent. When its resistance becomes comparable to that of the graphite emitter, V_{AB} starts to increase, V_{BC} saturates. The increase in V_{AB} is a self-consistent process. V_{AB} opens a gap in the embedded graphene bilayer, which causes the emitter resistance to increase, which increases V_{AB} further etc.
The calculation is done for tunnelling barriers ranging from 40nm to 200nm in width - see labels on the curves. The dashed line is the total bias V applied to the cell ($V=V_{AB}+V_{BC}$).

(iv) The ***I-V curves*** of the graphite-silicone tunnelling barrier are finally computed using Eq.S4. We calculate their dependence on p in Figure.2c. We calculate their dependence on temperature in Fig.S6. The temperature dependence of the peak position is plotted in Figure.3e.

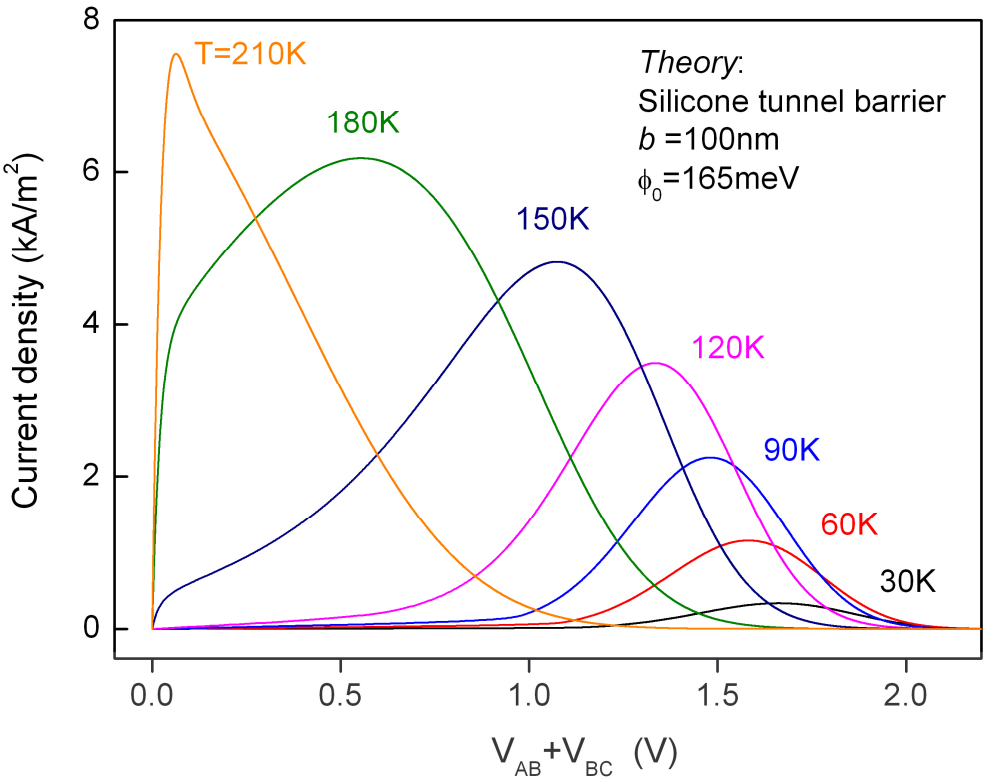

Figure S6 – **Theoretical temperature dependence of the I-V curves across the graphite-silicone tunnel barrier.**
This plot is used to compute the theoretical temperature dependence of the peak position in Figure.3e (red line). Increasing the temperature activates a thermal current which reduces the resistance of the barrier. The peak shifts to lower voltage as less bias is needed to bring the resistance of the barrier down to the level of the resistance of the emitter. The temperature dependence of the peak position gives an excellent fit to the experimental data in Figure.3e. The theory thus shows that the critical field F_p at which the composite fragments in electric field domains increases with decreasing temperature. Naturally the current through the barrier decreases with decreasing temperature due to the loss of the thermoactivated component. This effect competes with the rising current in the Ohmic regions of constant electric field. The experiment suggests that current continues increasing until the electric field reaches the value of F_p calculated with our model.

Our interpretation is summarized in Table S1 below:

	Before peak	**Above peak**
Silicone barrier	**Opaque**	**Transparent**
HOPG / PC	**Semimetal**	**Insulator**

Table S1 – **Crossover from silicone-controlled to graphite-controlled conduction.**

V TEMPERATURE DEPENDENCE OF THE I-V CURVES

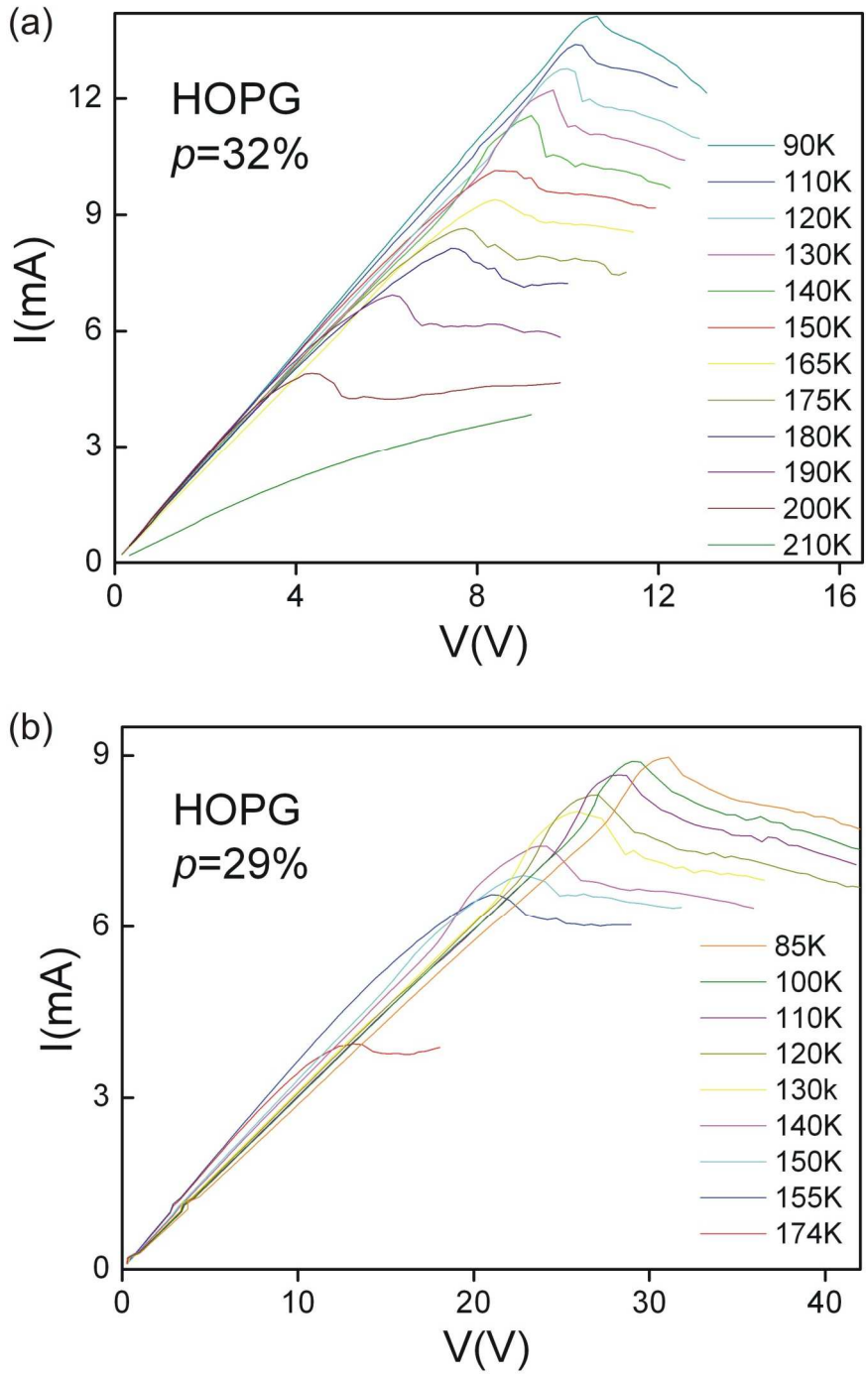

Figure S7 – **Temperature dependence of the I-Vs at two concentrations of HOPG in silicone.** (a) *p*=32%; (b) *p*=29%. The peak positions in panel (b) correspond to the open circles in Figure.3e.

VI. F.A.Q.s:

Q: Are the I-V curves reproducible when the bias voltage is cycled several times?

A: The I-V curves are very reproducible. The repeatability of the peak over 6 cycles is shown in Fig.S8.

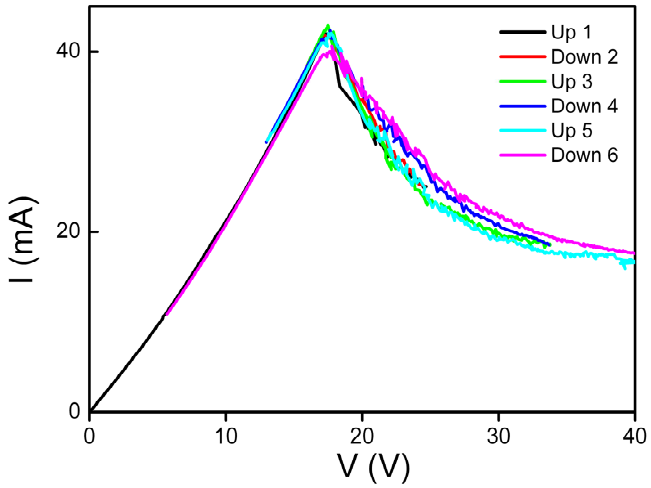

Figure S8 – Repeatability of the I-V curve of a HOPG-silicone composite over 6 bias cycles.

Q: Why are the I-V curves noisy after the peak?

A: After the peak, some percolation paths are switched-off and others are re-routed around the nanoparticles undergoing metal-insulator transition. These modifications to the conduction network will be accompanied by jumps in current that can explain the observed noise.

Q: Can the peak arise from Joule-induced melting of the silicone glass phase ?

A: To answer this point, we have measured Joule heating in-situ, using a Pt temperature sensor embedded inside the composite. The sensor was calibrated to within ±1°C and had an area of $1.2\times1.6mm^2$ (Microsens model from IST). We immersed the sample in liquid nitrogen and recorded the internal sample temperature while measuring the four terminal I-V curves. The results for the HOPG and PC composites are shown in Fig.S9.

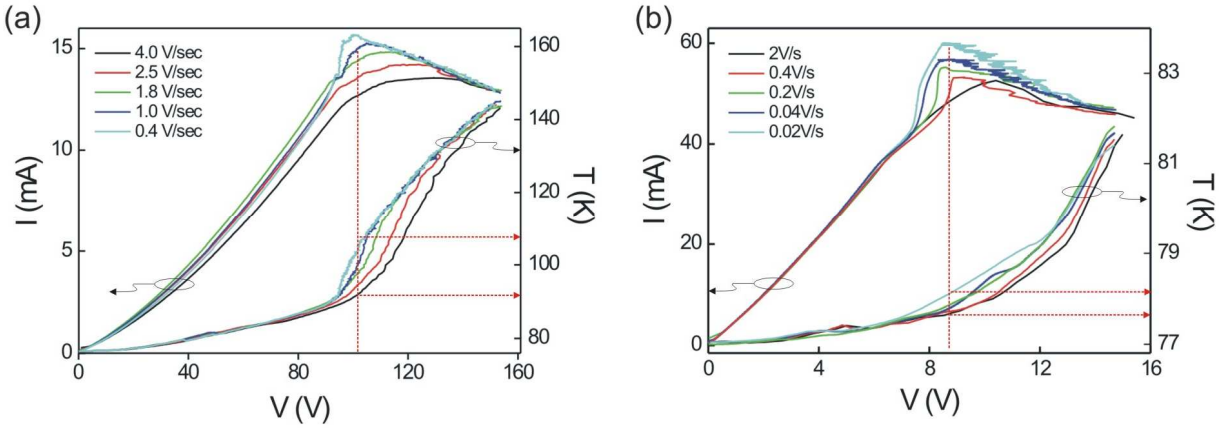

Figure S9 – Joule heating recorded in-situ during I-V curve measurements.

(a) HOPG composite, p=26%; (b) PC composite, p=29%.

The temperature measurements in Fig.S9 show some Joule heating in the HOPG sample and a smaller elevation of temperature in the PC sample. At the peak the temperature increases up to 92K-108K (HOPG) and 78K (PC). The glass transition of silicone rubber occurs at ~166K. We

conclude that ***Joule heating cannot raise the temperature sufficiently to the melt the glass phase of silicone***. ***The peak is not a heating effect.***

Another fact arguing against Joule heating is the observation that, in some samples, the Joule power dissipated at the peak is larger than that in the valley. For instance, the PC composite in Fig.1(c), dissipates 720mW (18V×40mA) at the peak and 650mW (42V×16mA) in the valley. Were Joule heating to melt the glass phase at the peak, the sample would vitrify again once the power drops below 720mW. This would cause the current to increase rather than drop – hence the ***Joule heating hypothesis is absurd***.

Q: Why not measuring composites at higher filling fractions (p>32%) ?

A: Mixing HOPG nanoparticles becomes difficult at filling fractions above 32%. The mixture forms lumps and becomes inhomogeneous. PC nanoparticles have a lower critical filling fraction. The critical filling fraction depends on the efficacy of the filler in lowering the surface tension of liquid silicone.

Q: The assumption of spherical nanoparticles to estimate the tunnelling barrier width is rough

A: The shape of individual nanoparticles becomes unimportant when ensemble averaging over the 100 million or so nanoparticles in the composite. Over-estimating (under-estimating) the tunnel barrier width will shift the current peak to higher (lower) bias voltage in Figure.2b without fundamentally affecting the NDR region.

Q: Why is the current peak sharper in PC composite ?

A: The random growth of graphene planes in annealed graphite makes it more likely that graphite planes tilted by 66° to 78° with respect to the electric field will form in ***each*** nanoparticle.

Q: Are electric field domains also present in the HOPG composite?

A: Yes – see Fig.S3c. The 0.4mm I-V curve has no NDR.

VII. BAND STRUCTURE OF BI- AND TRI-LAYER GRAPHENE

Self-consistent field-induced changes in isolated bi- and tri-layer graphene were found using the ab-initio CRYSTAL code[6], using both GGA and B3LYP hybrid exchange-correlation density functionals. Applied fields were $F=U/(ec)$ where c=0.335 nm and U=0.0, 0.5, 1.0 and 1.5 eV.

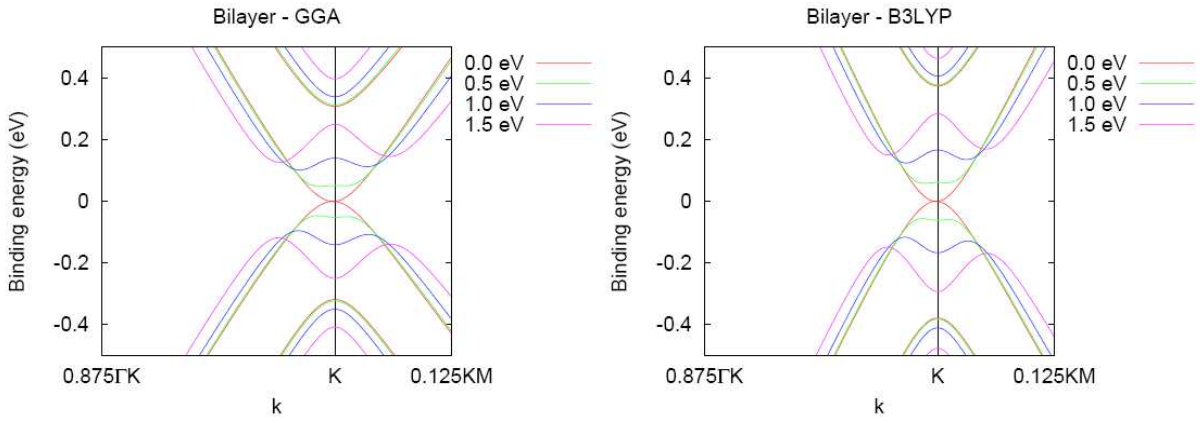

Figure S10 – Band structure of the AB graphene bilayer at different transverse biases.
The bias opens a gap at the Dirac point. The gap increases linearly with the bias up to 1.5V.

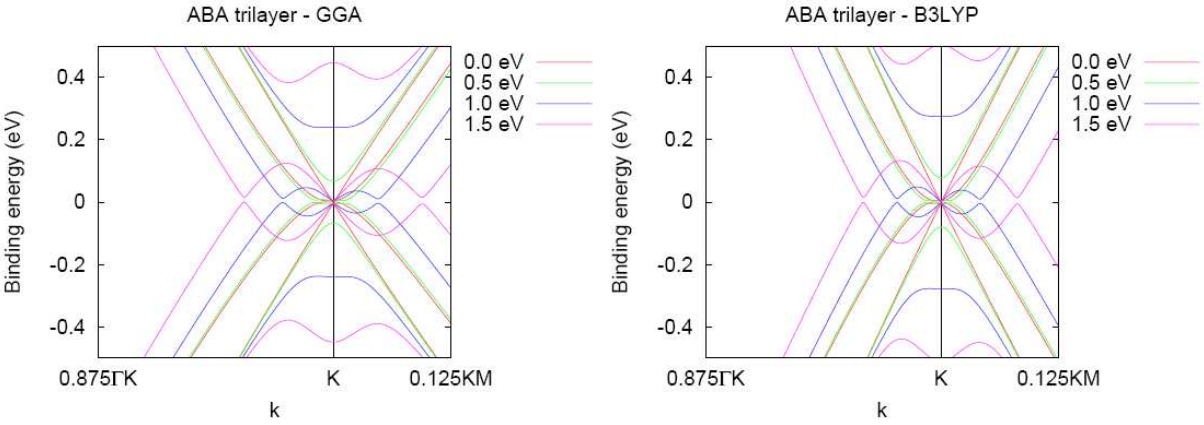

Figure S11 – Band structure of the ABA graphene trilayer at different transverse biases.
The ABA trilayer is gapless.

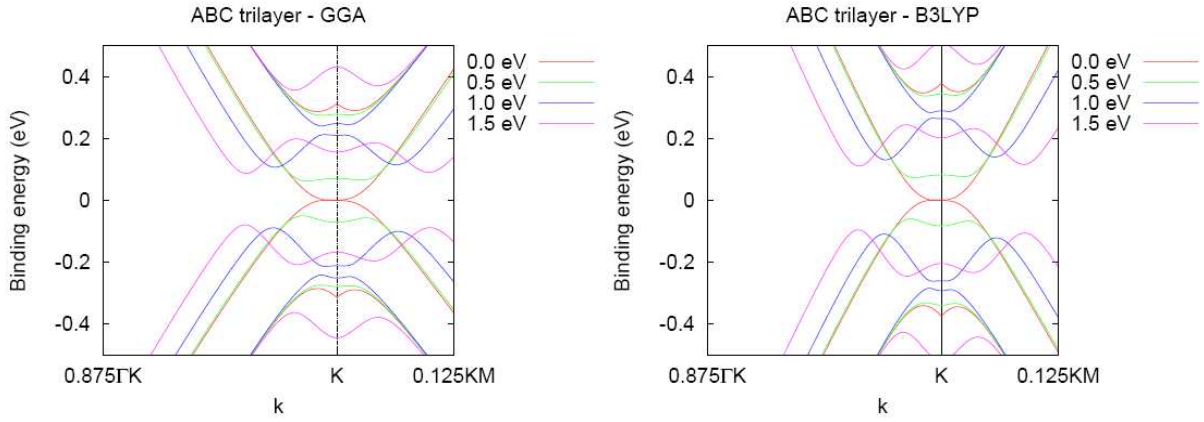

Figure S12 – Band structure of the ABC graphene trilayer at different transverse biases.
The ABC trilayer has an energy gap. The bias is applied to *neighbouring* graphene planes.

VIII. TIGHT BINDING MODEL

Non-self consistent tight-binding calculations are performed on thick slabs (96 and 97 layer slabs) assuming in-plane periodicity. Hamiltonian parameters are[7]:

γ_0 = 3.0 eV, in plane nearest neighbour interaction
γ_1 = 0.27 eV, nearest layer interaction between on-top atoms (type α)
γ_2 = -0.020 eV, next nearest layer interaction between type β atoms
Δ = 0.020 eV, on-site asymmetry between type α and type β atoms

Electric field effects were modelled using layer-dependent on-site shifts $U = \pm(V_{AB}/2)$, with the bias drop occurring across the central layers. The model applied to bi- and trilayer graphene gives generally similar band structures to the ab-initio methods (S10-S12) but for generally smaller U [8].

IX. DEFORMATION OF COMPOSITES

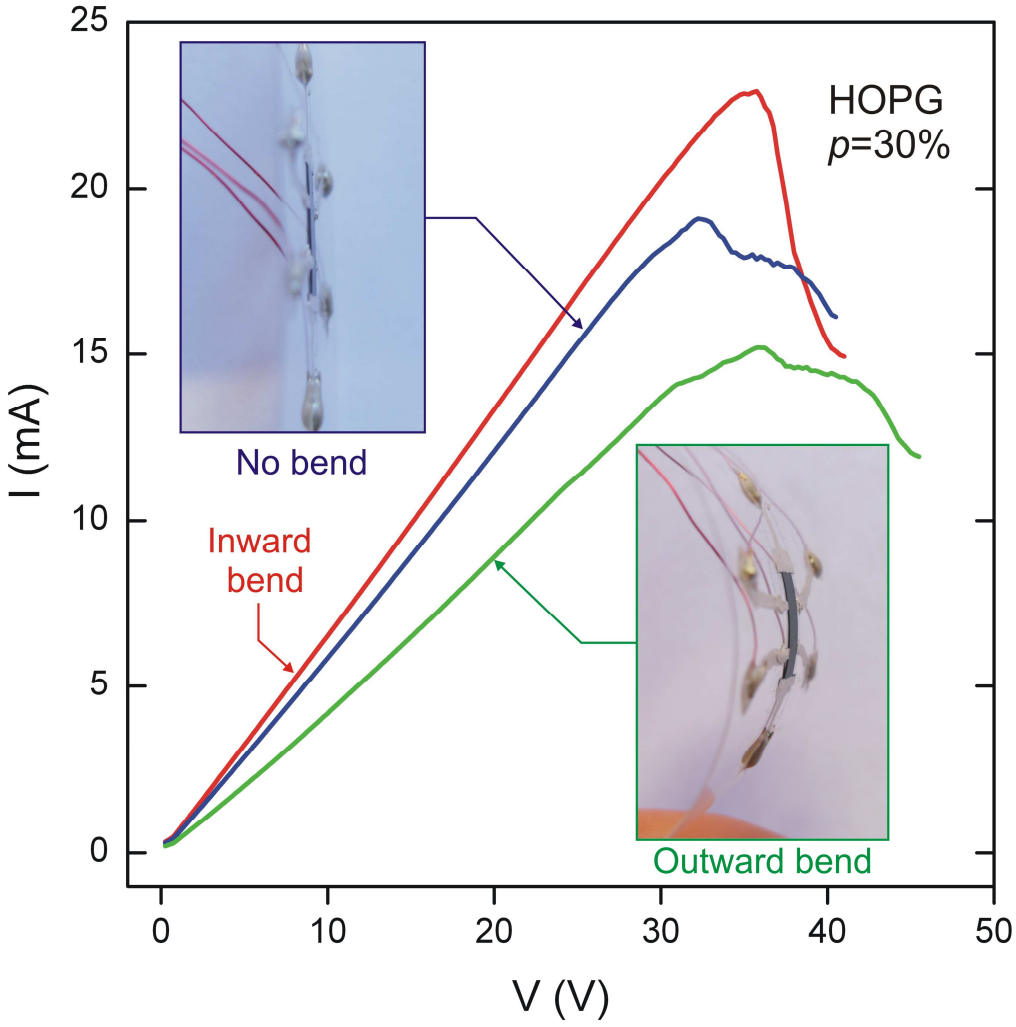

Figure S13 – Current-voltage characteristics of the bent composite.
A ribbon of composite is patterned on an acetate sheet which bends but does not stretch (inset). As a result, when the acetate sheet is bent inwards (resp. outwards) the composite is in compression (resp. tension). Putting the composite in compression has an effect similar to increasing the graphite filling fraction. The material is a flexible active composite because its NDR is robust under a relatively wide range of flexural conditions. Dimensions: ribbon length = 6mm, thickness = 0.15mm.

X REFERENCES:

[1] R. Tsu, L. Esaki, *Appl. Phys. Lett.* **1973**, *22*, 562.
[2] M. S. Dresselhaus, G. Dresselhaus, *Adv. in Phys.* **2002**, *51*, 1.
[3] A. H. Castro Neto, F. Guinea, N. M. R. Peres, K. S. Novoselov, A. K. Geim, *Rev. Mod. Phys.* **2009**, *81*, 109.
[4] K. S. Novoselov, E. McCann, S. V. Morozov, V. I. Fal'ko, M. I. Katsnelson, U. Zeitler, D. Jiang, F. Schedin, A.K. Geim, *Nature Phys.* **2006**, *2*, 177.
[5] K. Sugihara, K. Kawamura, T. Tsuzuku, *J. Phys. Soc. Jpn* **1979**, *47*, 1210.
[6] R. Dovesi, V. R. Saunders, C. Roetti, R. Orlando, C. M. Zicovich-Wilson, F. Pascale, B. Civalleri, K. Doll, N. M. Harrison, I. J. Bush, Ph. D'Arco, M. Llunell, **2006,** M. CRYSTAL06 User's manual, University of Torino, Torino.
[7] I. L. Spain, The electronic properties of graphite, in *Chemistry and Physics of Carbon* (P. L. Walker, Jr and P. A. Thrower, eds.) Vol. 8, Dekker, New York, **1973**, p1.
[8] Y. Zhang, T-. T. Tang, C. Girit, Z. Hao, M. C. Martin, A. Zettl, M. F. Crommie, Y. R. Shen, F. Wang, *Nature* **2009**, *459*, 820.